06

Defect structure, optical and photorefractive properties of $LiNbO_3:B:Gd$ single crystals

© I.V. Biryukova,[1] R.A. Titov,[1] I.N. Efremov,[1] V.V. Efremov,[1,2] L.A. Bobreva,[1] N.A. Teplyakova,[1] O.V. Palatnikova,[1] N.V. Sidorov,[1] M.N. Palatnikov[1]

[1] Tananaev Institute of Chemistry — Subdivision of the Federal Research Centre „Kola Science Centre of the Russian Academy of Sciences“,
184209 Apatity, Murmansk region, Russia
[2] Institute of North Industrial Ecology Problems Subdivision of the Federal Research Center „Kola Science Center of the Russian Academy of Sciences“,
184209 Apatity, Murmansk region, Russia
e-mail: r.titov@ksc.ru

Received March 14, 2025
Revised May 7, 2025
Accepted June 20, 2025

Technological approaches to obtaining nonlinear optical single-crystals of double doping $LiNbO_3:B:Gd$ have been investigated. It is shown that simultaneous doping with boron and gadolinium allows for targeted impact on the defect structure and practical properties of lithium niobate crystals. The solid-phase synthesis-granulation method helped to obtain the initial monophase charge of lithium niobate with a concentration of B_2O_3 of 0.03 mol.% and Gd_2O_3 of 0.62 mol.% corresponding to the composition of congruent melting. It has been found that the concentration of boron in the melt after growing $LiNbO_3:B:Gd$ crystals decreases by 3 times compared to its concentration in the initial charge. Two single crystals $LiNbO_3:(0.58\cdot10^{-3}\ B_2O_3):(0.51\ \text{mol.\%}\ Gd_2O_3)$ and $LiNbO_3:(0.32\cdot10^{-3}\ B_2O_3):(0.53\ \text{mol.\%}\ Gd_2O_3)$ were grown from a melt by the Czochralski method. Single crystals are similar in composition, and they are characterized by a low photorefractive effect, high compositional and optical uniformity. Both $LiNbO_3:B:Gd$ crystals are characterized by high Curie temperatures (1210 °C and 1213 °C). Using the method of IR absorption spectroscopy in the region of stretching vibrations of OH groups, it was shown that the increase in the concentration of hydroxyl groups in $LiNbO_3:B:Gd$ crystals is due to physicochemical and technological factors. Using laser conoscopy, it has been shown that the $LiNbO_3:(0.32\cdot10^{-3}\ B_2O_3):(0.53\ \text{mol.\%}\ Gd_2O_3)$ crystal has higher optical uniformity compared to the $LiNbO_3:(0.58\cdot10^{-3}\ B_2O_3):(0.51\ \text{mol.\%}\ Gd_2O_3)$ crystal.

Keywords: Lithium niobate, gadolinium, boron, double doping, laser conoscopy, photoinduced light scattering, IR absorption spectroscopy, optical microscopy.

DOI: 10.61011/TP.2025.11.62240.36-25

Introduction

The increasing demand for optical materials for laser radiation conversion determines the need to develop new and modify already used technological approaches aimed at improving the properties of nonlinear optical single crystals. Materials based on a nonlinear optical single crystal of lithium niobate ($LiNbO_3$) of various compositions with a unique combination of physical characteristics are among the most significant modern optical materials, which largely determine the development of such areas as optoelectronics, laser technology, integral and nonlinear optics [1,2]. The physical characteristics can be changed within a fairly wide range by varying the composition of the melt and crystal, as well as the defect state of the crystal by alloying and changing the stoichiometry. Materials based on lithium niobate single crystals of various compositions are also promising for holographic recording of information, for generating laser and terahertz radiation, for optical manipulation of micro- and nanoparticles, etc. [3–8].

In this regard, comprehensive studies are relevant aimed at studying the technological features of growing both nominally pure and doped single crystals $LiNbO_3$ in relation to the features of their structure, such as phases of variable composition, and physical characteristics. Such comprehensive studies create prerequisites for improving and scaling the technology of single crystals $LiNbO_3$, creating more advanced variants of growth equipment and technological methods of growing in order to obtain compositionally homogeneous optically perfect bulk single crystals of lithium niobate with desired properties by alloying with various combinations of dopant elements of various chemical nature.

According to the phase diagram in Ref. [4,9,10], lithium niobate is a nonstoichiometric oxygen-octahedral phase of variable composition with a wide range of homogeneity (from ~ 44.5 to ~ 50.5 mol.% Li_2O at 1460 K) and forms a continuous series of solid solutions. The congruent crystal composition ($LiNbO_{3cong}$), in which its composition is as close as possible to that of the melt, is characterized by a lack of lithium content ($R = [Li]/[Nb] = 0.946$). Due to the

peculiarities of the oxygen-polyhedral structure, consisting of oxygen-octahedral clusters of MeO_6 (Me — Li, Nb, impurity element, vacancy — V) connected by faces and edges, as well as small oxygen tetrahedra, which play the role of a peculiar „buffers" [11], lithium niobate is easily doped with metals [10,12–18]. In this case, the dopant metal is localized only in oxygen-octahedral clusters of the MeO_6 structure, violating the order of alternation of cations and vacancies along the polar axis existing in a nominally pure crystal $LiNbO_3$. During doping, the shape and lengths of interatomic bonds and the metal population of oxygen-octahedral clusters of MeO_6 change, which significantly affects the ferroelectric and nonlinear optical properties of the crystal $LiNbO_3$ and the state of its defective structure [4]. Moreover, concentration changes in the crystal defect state have a threshold character (concentration thresholds — CT). The mechanism of entry of the dopant element and the main (Li, Nb) elements into the crystal structure changes in the CT region [4,13,14]. The presence of CT does not lead to a phase transition and to a change in the spatial symmetry group characterizing the unit cell of the crystal, but the parameters of the unit cell of the crystal change due to changes in the lengths of interatomic bonds. Regulation of the physical characteristics of crystals $LiNbO_3$ by changing the state of its defective structure is currently one of the main approaches to creating new functional materials with specified physical characteristics.

Lithium niobate crystal is characterized by the photorefraction effect („optical damage"), at which the destruction of the laser beam in the crystal occurs and the accompanying photoinduced light scattering (PILS) [4,14], which limits its use as functional elements of optical devices for converting, modulating, and generating laser radiation. The enhancement of optical resistance of a single crystal $LiNbO_3$ to damage by laser radiation, i.e. minimization of local photoinduced changes in refractive indices and numerous photoinduced defects, is possible by introducing non-photorefractive metal cations into the crystal structure (Zn^{2+}, Mg^{2+}, In^{3+}, Gd^{3+} and others), which do not change their charge state under the influence of light, and, as a rule, the photorefraction effect is maximally suppressed when the concentrations of dopant non-photorefractive metals exceed the threshold values (more than ~ 5 mol.% of MgO and the order of ~ 7 mol.% of ZnO [13]) [4,14,19–21]. In this case, point defects of Nb_{Li} are completely displaced from the structure by dopant ions. However, at high concentrations of the dopant, the crystal, as a rule, becomes compositionally heterogeneous and is characterized by an increased concentration of macro- and microdefects of various kinds, as well as the presence of impurity phases [22]. At the same time, a noticeable suppression of the photorefractive effect in $LiNbO_3$ crystals is already observed at a low concentration of alloying metals. In particular, for the crystal of $LiNbO_3:Gd$ — at ~ 0.05 mol.% of Gd_2O_3 [16]. It should be noted that at low concentrations, divalent and trivalent cations of non-photorefractive metals (Zn^{2+}, Mg^{2+}, Gd^{3+}, etc.) are localized in lithium octahedra of an ideal crystal structure. At the same time, they can arrange the cationic sublattice of the crystal, increasing its optical quality [4,23].

The introduction of rare earth elements (REE) into the crystal structure $LiNbO_3$, in addition to reducing the effect of photorefraction, also enables photoluminescence and, in some cases, laser generation. The emission properties of crystals $LiNbO_3:REE$ are determined by the type and concentration of REE, the mechanism of their entry into the structure, as well as the features of the defective structure formed during the growing of crystals [17]. The review in Ref. [17] discusses in detail the effect of various dopant elements, including REE, on the properties of crystals $LiNbO_3$.

An important characteristic of a ferroelectric crystal is the Curie temperature (T_C), which to a certain extent reflects its structural perfection. The more perfect the crystal structure, the higher the Curie temperature. T_C for a single crystal of $LiNbO_{3cong}$ is $\sim 1145\,^\circ C$ [24], T_C decreases to $\sim 1135\,^\circ C$ for single crystals of $LiNbO_3:Gd$ with an increase in the concentration of Gd in the melt from ~ 0.05 mol.% to 0.5 mol.% of Gd_2O_3 [23]. The main factor influencing the type of concentration dependences T_C in lithium niobate crystals doped with metallic impurities are the positions of the main (Li and Nb) and impurity cations in the structure and their valence, which determine the number of vacancies and, accordingly, the perfection of the cationic sublattice [23]. Thus, a decrease in T_C indicates a decrease in the structural perfection of the cationic sublattice of lithium niobate crystals, including due to the possibility of localization of niobium cations and alloying metal impurity cations in vacant octahedra of the lithium niobate structure [25]. On the contrary, an increase in T_C indicates an increase in the structural perfection [23], including due to a decrease in the concentration of point defects Nb_{Li} producing four lithium vacancies V_{Li}, which are electron traps responsible for the effect photorefraction in a lithium niobate crystal. It should also be noted that when several metallic impurities are introduced into a crystal (double or triple doping) or the same impurity is localized in different positions of the cationic sublattice, mutual compensation of the ordering and disordering mechanisms of the impurity action is possible [4]. Thus, in relation to T_C, the additivity of the effect of dopant components can be observed [26].

A fundamentally different mechanism of indirect effect on the state of the defective structure of the lithium niobate crystal is provided by the introduction of a chemically active nonmetallic element — boron into the melt, which is a kind of „moderator" of the melt. It changes the physico-chemical properties and structure of the melt and, thus, changes the defective structure of the growing lithium niobate single crystal. In this sense, boron is a unique dopant additive: it practically does not enter the crystal, but as an active complexing agent, changing the structure and properties of the melt, it changes the state of structural defects and properties of the crystal $LiNbO_3$. However,

crystals $LiNbO_3:B$ with increasing boron concentration in the melt are characterized by defects such as „channels", which are hollow channels in the crystal volume [24]. In this regard, the identification of the optimal concentration of boron in the initial melt during the growing of lithium niobate crystals by the Chokhralsky method in order to determine the optimal limits of the permissible concentration of boron, which avoids the formation of this type of defects, is an urgent technological task. It should be noted that the effect of boron on the melt structure and the state of the defective structure of lithium niobate single crystals has not been sufficiently studied to date. A review of the few studies devoted to this topic is presented in Ref. [24], where it is shown that low concentrations of boron in the melt reduce the defect of the lithium niobate crystal. At the same time, other non-metallic elements with increasing concentration have a rather negative effect on the structural perfection of the lithium niobate crystal. Thus, the effect on the properties of a lithium niobate crystal of phosphorus or silicon leads to the formation of cracks and extended areas of optical inhomogeneity [27].

Boron, as a strong complexing agent, affects the composition and structure of complex ionic complexes in the melt: the ionic complexes in the melt become larger when boron is introduced into it, and the number of complex types decreases. This contributes to the production of lithium niobate single crystals with a higher degree of optical uniformity [24]. Along with this, boron binds niobium excess in the melt congruent composition into strong niobium-containing complexes, which contributes to the approximation of the crystal composition to the stoichiometric $(R = [Li]/[Nb] \approx 1)$ [24]. Thus, crystals of $LiNbO_3:B$ grown from a boron-containing melt of congruent composition are characterized by a lower concentration of point defects of Nb_{Li} compared to crystals of $LiNbO_{3cong}$. Consequently, the composition of crystals $LiNbO_3:B$ is approaching stoichiometric, and their structural, compositional, optical uniformity and resistance to laser damage are noticeably increased [24]. It has already been shown that T_C of $LiNbO_3:B$ crystals are significantly higher than those of $LiNbO_{3cong}$ crystals ([24]), which indicates a decrease in the number of lithium vacancies and, accordingly, increasing the degree of structural perfection of the cationic sublattice of boron-containing crystals [24]. It should also be noted that the addition of a strong complexing agent — boron to the melt can lead to a decrease in the CT value of the metallic impurity [28]. Therefore, it is possible to significantly reduce the concentration of the dopant metal, at which there is a strong increase in the resistance of crystals to damage by laser radiation. This also makes it possible to significantly increase the optical uniformity of doped lithium niobate crystals.

In recent years, the attention of researchers has been attracted by double doping crystals of $LiNbO_3$ [4,16,28–33]. In particular, double doping crystals of $LiNbO_3:B:Gd$ are of interest for the development of optical materials for the conversion of laser radiation. In crystals of $LiNbO_3:B:Gd$, the non-photorefractive metallic impurity Gd^{3+} reduces the photorefractive effect, the non-metallic impurity B^{3+} also reduces the photorefractive effect, but the element B^{3+} increases the optical and compositional uniformity of the lithium niobate crystal. In addition, double doping simultaneously with two „non-photorefractive" cations (Gd^{3+} and B^{3+}) makes it possible to more finely regulate the ordering of structural units of the cationic sublattice and the polarizability of oxygen-octahedral clusters of MeO_6, which determine the amount of spontaneous polarization and the nonlinear optical properties of the crystal $LiNbO_3$. This double doping also makes it possible to fine-tune the type and number of point and complex defects with electrons localized on them, which determine the magnitude of the photorefraction effect. Thus, double doping opens up the potential for a more subtle and targeted effect on the features of the defective structure and practically significant properties of lithium niobate crystals.

Double doping of a crystal $LiNbO_3$ with a metallic element Gd^{3+} and a nonmetallic element B^{3+} is a new approach to creating functional materials with high compositional and optical uniformity. In this case, metallic impurities are localized in the crystal structure $LiNbO_3$ only in octahedral positions, while the nonmetallic element boron is unable to localize in oxygen-octahedral clusters of MeO_6 structures [24]. The boron element is localized in the crystal structure $LiNbO_3$ in trace amounts ($\sim 10^{-4}$ wt.%) in small tetrahedral voids of the structure [24]. It should be noted that there are few studies in the literature of lithium niobate crystals of double doping, when metal and nonmetal act as dopants [28]. In this regard, the task of obtaining optically highly perfect double-doped crystals of $LiNbO_3:B:Gd$ is relevant and in important from both fundamental and applied points of view. Such crystals may be promising as optical materials for converting laser radiation.

The analysis of the melt features of the $Li_2CO_3:Nb_2O_5:Gd_2O_3:H_3BO_3$ system is performed in this paper based on the literature data, which is necessary for obtaining non-photorefractive single crystals of $LiNbO_3:B:Gd$ of high compositional uniformity with optimal concentrations of dopant elements, and the results of complex studies of the features of defective macro- and microstructure and photorefractive properties by optical microscopy, IR absorption spectroscopy in the field of valence vibrations of hydrogen atoms of OH groups, differential thermal analysis (DTA), laser conoscopy and photoinduced light scattering (PILS) of double doping single crystals of $LiNbO_3:(0.58 \cdot 10^{-3}\ B_2O_3):(0.51$ mol.% $Gd_2O_3)$ and $LiNbO_3:(0.32 \cdot 10^{-3}\ B_2O_3):(0.53$ mol.% $Gd_2O_3)$. These single crystals were obtained by us for the first time and have not been previously studied in the literature.

1. Experimental procedure

The use of boron-containing lithium niobate melts requires fundamentally different approaches in comparison with the conditions for obtaining pure or doped with metallic impurities of lithium niobate. This concerns both the choice of the method of synthesis of the initial charge and the optimization of the processes of growing single crystals by the Chokhralsky method [24]. A granular charge of lithium niobate of congruent composition doped with boron and gadolinium was obtained by solid-phase synthesis-granulation from a mixture of extremely pure $Li_2CO_3:Nb_2O_5:Gd_2O_3:H_3BO_3$. The main components of the mixture were subjected to preliminary heat treatment: lithium carbonate $Li2CO_3$ was annealed at a temperature of 250 °C for 3 h, niobium pentoxide Nb_2O_5 was annealed for 5 h at a temperature of 1100 °C. The calculation of the required amount of lithium carbonate, providing a congruent ratio of the main components, was carried out taking into account the content of Gd_2O_3 in the initial mixture and without taking into account the amount of boric acid due to its low content in the charge. After mechanical activation of the reagents for 24 hours, the mixture was placed in a platinum crucible and lightly pressed in a fluoroplastic mixer „drum tumbler". The heat treatment was carried out in a PVK-1.4-25 annealing furnace. The granulation temperature and the holding time of the mixture were selected experimentally and taking into account the studies presented in Ref. [24].

X-ray diffraction analysis (XRD) of the charge $LiNbO_3:B:Gd$ was performed by powder diffraction method using XRD-6000 (Shimadzu, Japan) with the powder diffraction database PDF-4 2021 (ICDD, USA). Single crystals of lithium niobate $LiNbO_3:(0.58\cdot10^{-3}$ $B_2O_3):(0.51$ mol.% $Gd_2O_3)$ and $LiNbO_3:(0.32\cdot10^{-3}$ $B_2O_3):(0.53$ mol.% $Gd_2O_3)$ were grown in the (001) direction by the Chokhralsky method from platinum crucibles with a diameter of 80 mm in an air atmosphere on an induction-type growth unit „Crystal 2" equipped with an automatic crystal diameter control system. The design of the heat node provided a combination of an axial temperature gradient over the melt ~ 1 deg/mm and an extended isothermal region in the zone of post-cold annealing of the crystal. The formation of a flat crystallization front was ensured by a displacement velocity of 0.8 mm/hour and a rotation velocity of 8 rpm. The full load of the crucible was ~ 1510 g. At the same time, no more than ~ 17 % of the melt was spent for growing each crystal.

The grown single crystals of $LiNbO_3:B:Gd$ were subjected to thermal annealing at $T = 1235$ °C for 15 h in a high-temperature annealing furnace PVK-1.4-25 to relieve thermoelastic stresses. The heating and cooling rate was 50 deg/hour.

0.8 mm thick plates were cut from the upper (cone) and lower (bottom) parts of the crystal boule to prepare powder samples to determine the concentration of impurities B and Gd in $LiNbO_3:B:Gd$ crystals. The concentration of dopants in the charge, $LiNbO_3:B:Gd$ crystals and melt remaining after crystal growth was determined by inductively coupled plasma mass spectrometry using an ELAN 9000 DRC-e quadrupole mass spectrometer with measurement accuracy up to $1\cdot10^{-7}$.

Studies of the macro- and microdefect structure of lithium niobate crystals doped with boron and gadolinium were carried out on plates with a thickness of 1 mm Z-cut using optical microscopy using the „Thixomet" image analysis system, including the „Carl Zeiss„ Axio Observer.D1m optical microscope docked via a „PixeLink PL-B774U" digital video camera with a computer equipped with the „ThixometPRO" program in light field modes and the differential interference contrast method. For comparison, a crystal of $LiNbO_3:Gd$ with a similar concentration of gadolinium of 0.42 mol.%, was previously grown under similar conditions in crystal. The plates were cut from the crystals of $LiNbO_3:B:Gd$ and $LiNbO_3:Gd$ after heat treatment, they were ground, polished and chemically etched at room temperature for 20 h in a mixture mineral acids $HF:HNO_3 = 1:3$.

The reduction to a single-domain state of $LiNbO_3:B:Gd$ crystals was performed by high-temperature electrodiffusion annealing (HTEDA) in a „Lantan" furnace with cooling of samples at a rate of 20 deg/hour in the temperature range from 1235 °C to 735 °C under a constant electric field.

The degree of unipolarity of single crystals of $LiNbO_3:B:Gd$ was controlled by studying the static piezoelectric effect. The method for determining the piezo module (d_{333}) is presented in Ref. [24].

The optical purity of the material was estimated by the number of scattering centers per unit volume of a single-crystal boule according to the method presented in Ref. [24].

Optical transmission spectra in the visible region were recorded using a UVI-256 spectrophotometer manufactured by LOMO (St. Petersburg, Russian Federation). The study also used carefully polished crystal plates of $LiNbO_3:B:Gd$ and $LiNbO_3:Gd(0.42$ mol.% $Gd_2O_3)$ of Z-orientations with a thickness of ~ 1 mm.

Synchronous thermal analysis of the samples was performed using HQT-4 equipment (Beijing Henven Experimental Equipment Co., Ltd., China, 2022) in platinum crucibles at a heating rate of 20 deg/min. Argon was used as a purge gas (flow rate 100 ml/min). An empty crucible was used for comparison. The sample was heated in the temperature range of $\sim$ from 30 °C to 1400 °C. The weight of the suspension was ~ 20 mg. The sample was weighed on an analytical scale CAS CAUW 120D Ver. NO 2.3.3 (CAS Corporation, South Korea, 2022) with an accuracy of 0.01 mg.

IR absorption spectroscopy in the field of valence vibrations of OH groups was used to identify and quantify defects in the form of hydroxyl OH groups in crystals of $LiNbO_3:B:Gd$. The crystal of $LiNbO_{3cong}$ was chosen as the object of comparison. IR absorption spectra were recorded using a Nicolet 6700 Fourier spectrometer (Thermo Fisher Scientific Inc., Hillsboro, OR, USA, 2010).

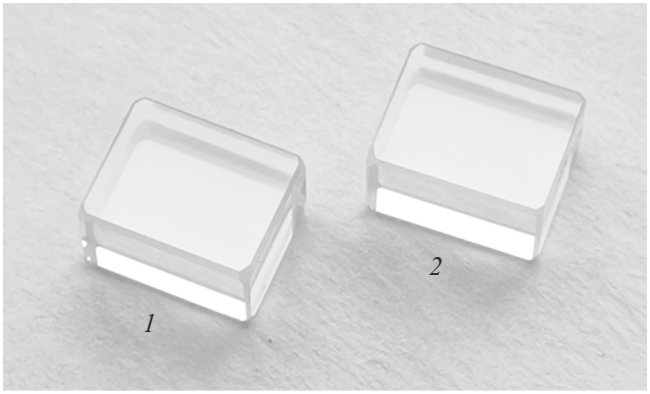

Figure 1. Samples of single crystals of $LiNbO_3:(0.58\cdot10^{-3}$ $B_2O_3):(0.51$ mol.% $Gd_2O_3)$ — (*1*) and $LiNbO_3:(0.32\cdot10^{-3}$ $B_2O_3):(0.53$ mol.% $Gd_2O_3)$ — (*2*).

The measurements were performed with unpolarized infrared radiation at room temperature. The range of recorded wavelengths was $4000-400\,cm^{-1}$. The volume concentration of OH groups in the studied crystals was determined using the Clavier method [34]. We used LabSpec 5.5 and Origin 8.1 programs to process the experimental data and determine the main parameters of spectral lines from the IR spectra of the studied samples (parallelepipeds with dimensions $8\times6\times10$ mm, the edges of which coincided in the direction with the crystallographic axes $X\times Y\times Z$, and the faces were carefully polished (Fig. 1)).

532.0 nm Nd:YAG laser (MLL-100, Changchun New Industries Optoelectronics Tech. Co. Ltd, Changchun, China) with a power of 1 and 90 mW (for laser conoscopy) and a power of 160 mW (PILS, with a power density of $6.3\,W/cm^2$) was used to obtain conoscopic images by laser conoscopy and in photoinduced light scattering experiments (PILS). A detailed methodology is given in Ref. [35]. 3 mm thick plates were used to obtain conoscopic patterns by laser conoscopy of $LiNbO_3:B:Gd$ crystals, and parallelepipeds were used to obtain PILS patterns (Fig. 1).

2. Results and discussion

2000 g batch of granular charge with a bulk weight of $2.8\,g/cm^3$ was obtained. The granulation temperature and the holding time of the mixture were selected experimentally: the mixture was heated at a rate of 350 deg/hour to 1150 °C, then at a rate of 90 deg/hour to 1239 °C, followed by exposure at this temperature for 5 h. The content of dopants was: 0.03 mol.% B_2O_3 ($24\cdot10^{-4}$ wt.%); 0.62 mol.% Gd_2O_3 (0.65 wt.%). According to the XRD data the charge of $LiNbO_3:B:Gd$ was monophasic and was identified by the ICDD card № 04-015-9601.

A special feature of this charge is the combination of a light non-metallic element B ($M_r = 10.811$ g/mol), which acts simultaneously as an dopant component of both the flux and the heavy rare earth element Gd ($M_r = 157.25$ g/mol). Due to the different chemical nature of the dopant elements, the melt was homogenized by significantly overheating it (by 200 °C) above the melting point of lithium niobate, exposure for 8 h, and subsequent rapid cooling to the seeding temperature. This approach contributes to the destruction of associative bonds in the lithium niobate melt [24], freeing from gas inclusions and stabilizing the properties of the melt.

Two crystals were grown under the same thermal conditions and technological conditions: $LiNbO_3:(0.58\cdot10^{-3}$ $B_2O_3):(0.51$ mol.% $Gd_2O_3)$ and $LiNbO_3:(0.32\cdot10^{-3}$ $B_2O_3):(0.53$ mol.% $Gd_2O_3)$ (next — crystals $LiNbO_3:B:Gd(1)$ and $LiNbO_3:B:Gd(2)$, respectively) with a diameter of ~35 mm and the length of the cylindrical part ~55 and ~45 mm, the weight ~247 and 208 g, respectively. After growing the first crystal, an doped charge of $LiNbO_3:B:Gd$ was loaded into the crucible in an amount equal to the weight of the grown single crystal.

The results of inductively coupled plasma mass spectrometry analysis of the content of dopant components in the cone (C_c) and bottom (C_f) parts of single crystals of $LiNbO_3:B:Gd$(1 and 2) are given in Tables 1, 2. The calculation of the initial gadolinium concentration in the melt during the growth of the second single crystal and the distribution coefficient (K_D) was performed according to the method presented in Ref. [13].

The concentration of gadolinium on the surface and in the volume of the melt after growing a single crystal of $LiNbO_3:B:Gd(2)$ was 0.76 mol.% and 0.73 mol.% Gd_2O_3, respectively, which is typical for the impurity distribution in the case of K_{0eff} less than unity [36]. However, the crystals of $LiNbO_3:B:Gd$(1 and 2) have a high degree of chemical uniformity: the change in gadolinium concentration along the length of the boule for the crystal $LiNbO_3:B:Gd(1)$ is -0.01 mol.% Gd_2O_3, for crystal $LiNbO_3:B:Gd(2)$ — -0.02 mol.% Gd_2O_3 (table. 1), which is more consistent with the nature of the dopant distribution at $K_{0eff}=1$.

The concentration of boron on the surface and in the volume of the melt after growing a single crystal of $LiNbO_3:B:Gd(2)$ was 0.01 mol.% and 0.007 mol.% B_2O_3, respectively, which is approximately three times less than the initial concentration of boron in the charge (0.03 mol.% B_2O_3). At the same time, the boron content in the crystal of $LiNbO_3:B:Gd(2)$ is approximately two times less than in the crystal $LiNbO_3:B:Gd(1)$ (Table 2).

The distribution of boron along the growth axis of $LiNbO_3:B:Gd(1)$ crystal is fairly uniform: the concentration difference is 0.00001 mol.% B_2O_3. For a $LiNbO_3:B:Gd(2)$ crystal grown under similar conditions, the boron content in the cone part of the boule is lower than in $LiNbO_3:B:Gd(1)$ crystal, and decreases to its end (Table 2). In general, taking into account the insignificant concentration of boron included in the crystal structure, it can be argued that the selected thermal conditions and technological modes of growth of crystals of $LiNbO_3:B:Gd$(1 and 2) are correct.

Table 1. Concentration of Gd in the initial melt ($[Gd]_L$), cone and bottom parts of the grown single crystals of $LiNbO_3:B:Gd$ ($[Gd]s$), change in gadolinium concentration along the length of the bead (ΔC_{Gd}) and gadolinium distribution coefficient (K_{DGd}).

Crystals $LiNbO_3:B:Gd$	Concentration of Gd, mol.%				K_{DGd}
	$[Gd]_L$	$[Gd]_s$ in the cone	$[Gd]_s$ in the bottom	$\Delta C_{Gd} = C_c - C_b$	
№ 1	0.62	0.51	0.52	−0.01	0.82
№ 2	0.64	0.53	0.55	−0.02	0.83

Table 2. Boron concentration in the cone and bottom parts of single crystals ($[B]_s$, mol.%) grown from a charge containing 0.03 mol.% B_2O_3 and 0.62 mol.% Gd_2O_3, and the change in boron concentration along the length of the boule (ΔC_B)

Crystals $LiNbO_3:B:Gd$	Concentration B, mol.%		
	$[B]_s$ in the cone	$[B]_s$ in the bottom	$\Delta C_B = C_c - C_b$
№ 1	0.00058	0.00057	0.00001
№ 2	0.00032	0.00024	0.00008

According to the phase diagram of the system Li_2O–Nb_2O_5–B_2O_3, boron should not enter the structure of the lithium niobate crystal, since the phase $LiNbO_3$ does not have the solubility range of boron in the solid state [37]. Boron enters the crystal structure $LiNbO_3:B$ at the level of trace amounts [24]. The reason for the decrease in the boron concentration in $LiNbO_3:B:Gd(2)$ crystal may be a prolonged but necessary overheating of the melt before growing a single crystal, which, combined with an initially low concentration of boron in the charge (0.03 mol.% B_2O_3) leads to intensive evaporation of nonmetals during the growth of single crystals. This is confirmed by a decrease in the boron content in the melt volume.

The optical quality of crystals of $LiNbO_3:B:Gd(1$ and $2)$ was evaluated by the number of scattering centers in the crystal volume. The presence of scattering centers in crystals is caused by microdefects of the structure, which look like individual luminous dots or clusters of them in the laser beam. The appearance of scattering centers can be caused, among other things, by the presence of a residual domain structure in crystals after the transition to a single-domain state. There are almost no point and extended defects in the form of scattering centers in the single crystal of $LiNbO_3:B:Gd(1)$. The average density of microdefects in the form of scattering centers is $\sim 7.22\,cm^{-3}$ in a single crystal of $LiNbO_3:B:Gd(2)$. Thus, both crystals meet the requirements for optical quality crystals (the average density of scattering centers is less than $10\ cm^{-3}$).

A grown polydomain lithium niobate single crystal in its initial state (before undergoing the transition to a single-domain state), as a rule, does not have a piezoelectric effect. In this case, the macroscopic characteristic of piezoelectric properties is the magnitude of the components of the piezoelectric tensor, including the magnitude of the piezo module, $d_{333} \approx 0$. HTEDA leads to the appearance of a distinct piezoelectric response in lithium niobate crystals. Fig. 2 shows, as an example, the dependence of the polarization charge Q_p on the force applied in the direction of the polar axis of the crystal F after the HTEDA for crystals of $LiNbO_3:B:Gd(1$ and $2)$. According to the results of three measurements, the piezoelectric module d_{333} of a single crystal of $LiNbO_3:B:Gd(1)$ was $\sim 7.02 \cdot 10^{-12}$ C/N (Fig. 2, *a*). This indicates a relatively high degree of unipolarity of $LiNbO_3:B:Gd(1)$ crystal. It is possible to achieve a higher value of the piezomodule by adjusting the temperature range of the electric field application and the HTEDA modes.

The average value of the piezoelectric module d_{333} for $LiNbO_3:B:Gd(2)$ crystal is slightly lower than for $LiNbO_3:B:Gd(1)$ crystal, and is $\sim 6.87 \cdot 10^{-12}$ C/N (Fig. 2, *b*). This may be due to a slight increase in the gadolinium concentration in $LiNbO_3:B:Gd(2)$ crystal (Table 1). Moreover, the graph of the dependence $Q_p = f(F)$ of $LiNbO_3:B:Gd(2)$ crystal shows jumps in the polarization charge Q_p and some deviation of the graphs from linearity, which indicates the influence of the electric field created by the load for residual microdomains and unbalanced charges remaining after undergoing the reduction to a single-domain state. The study of the microstructure of these crystals in comparison with the crystal of $LiNbO_3:Gd(0.42$ mol.% $Gd_2O_3)$ obtained by direct doping was performed by optical microscopy and is given below.

Structural defects in crystals $LiNbO_3$ can be divided into growth and technological defects according to the stage of their appearance in the process of obtaining crystalline material. The first type of defects are defects that occur directly during the growth of lithium niobate crystals due to the thermodynamic properties of the melt-growing crystal system. The number and configuration of such defects depends on the thermodynamic features of the crystallization process, and, accordingly, on the type of initial components, thermal and kinetic growing conditions, the thermal history of the melt and its chemical composition. The macro- and microdomain structure of lithium niobate crystals, which occurs during the phase transition of the crystal from a paraelectric to a ferroelectric state, as well as the substructure of the crystal, is directly

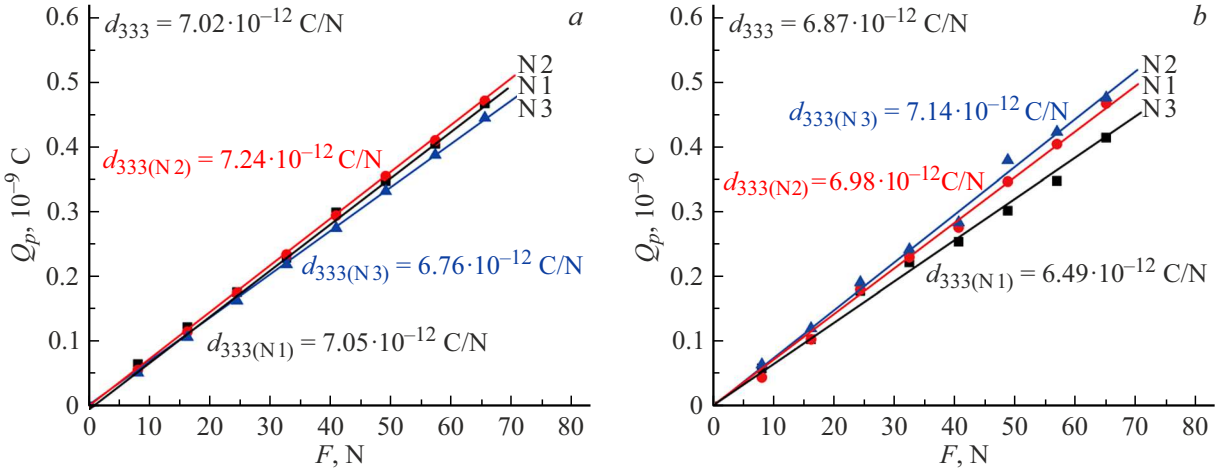

Figure 2. Dependence $Q_p(F)$ for crystals: $LiNbO_3:B:Gd(1)$ — *a*; $LiNbO_3:B:Gd(2)$ — *b*.

related to the growth defect structure. The change in the growth defect structure of crystals $LiNbO_3$ occurs as a result of post-growth thermal and electrothermal treatment. Such treatment is usually accompanied by a significant transformation of the growth defect structure (point and extended defects, dislocations, macro- and microdomains, macro- and microdomain boundaries, block substructure, segregation of impurities, inclusions of the second phase, etc., etc.) up to the complete disappearance of some types of defects. Thus, the piezoelectric module d_{333} of crystals of $LiNbO_3:B:Gd$ after transition to a single-domain state increased from ~ 0 to $\sim 7 \cdot 10^{-12}$ C/N (Fig. 2), which is attributable to the disappearance of most of the growth domain macro- and microstructure during electrothermal treatment. During post-treatment, new types of structural defects may occur, the number and configuration of which are determined by the technological parameters of the thermal and electrothermal treatment processes, the type and concentration of dopants. Such defects that occur during the transformation of a growth defect structure or are newly formed as a result of post-growth thermal and electrothermal treatment and, as a rule, are absent in as-grown crystals $LiNbO_3$ that have not been subjected to post-growth treatment can be conventionally called technological.

Optical microscopy study of the macro- and microstructure of as-grown crystals of $LiNbO_3:B:Gd(1$ and $2)$ in comparison with the crystal of $LiNbO_3:Gd(0.42$ mol.% $Gd_2O_3)$ before conversion to the single-domain state, made it possible to evaluate the effect of the presence of boron in the melt on the configuration of the growth macro- and microdefect structure of $LiNbO_3:B:Gd$ crystals. In the case when the distribution coefficients of dopant additives are noticeably less than unity and radically differ in magnitude (Tables 1, 2), additional information on the mechanisms of crystal growth is extremely important, depending on the type and concentration of dopant additives. Moreover, the type of macro- and micro-defective crystal structure allows us to obtain additional information about the physico-chemical characteristics of the crystal-melt system and the mechanisms of crystallization. Fig. 3 shows the macro- and microstructure of the crystal $LiNbO_3:Gd(0.42$ mol.% $Gd_2O_3)$.

The domain structure of X-cut of $LiNbO_3:Gd$ crystals is similar to the domain structure of lithium niobate crystals doped with any other rare earth impurities. Thus, the macrostructure of the crystal $LiNbO_3:Gd(0.42$ mol.% $Gd_2O_3)$ of the X-cut is formed by growth bands with complex rugged domain boundaries. A fragment of such a growth band is shown in Fig. 3, *a*. The crystal $LiNbO_3:Gd(0.42$ mol.% $Gd_2O_3)$ is highly prone to cracking.

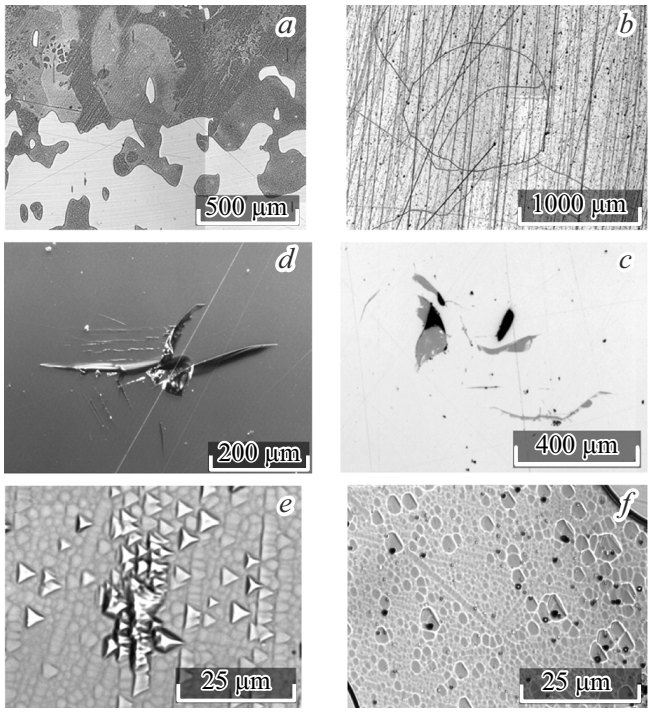

Figure 3. Macro- and microstructure of the crystal of $LiNbO_3:Gd(0.42$ mol.% $Gd_2O_3)$ X (*a*) and Z-cut (*b*–*f*).

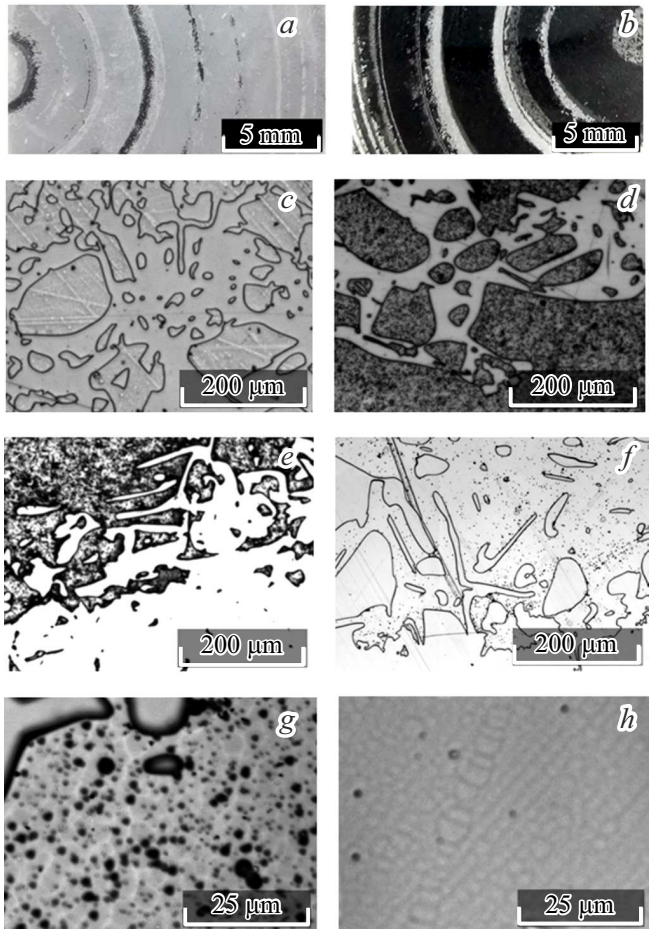

Figure 4. Macro- (*a–f*) and microstructure (*g*, *h*) crystals of $LiNbO_3:B:Gd(1)$ (left column) and $LiNbO_3:B:Gd(2)$ (right column) before the HTEDA procedure.

Thus, significant areas are observed on the Z-cut of the crystal, occupied by stress grids (Fig. 3, *b*), chips, cracks and lacunae (Fig. 3, *c*, *d*), clusters of triangular domains against the background of the second phase (Fig. 3, *e*). The cells of the substructure of crystal $LiNbO_3:Gd(0.42\,\text{mol.}\%\ Gd_2O_3)$ vary greatly in size and shape, and microdomains of the opposite sign are clearly fixed against their background (Fig. 3, *f*). All this indicates a highly stressed state of the crystal $LiNbO_3:Gd(0.42\,\text{mol.}\%\ Gd_2O_3)$.

Unlike crystals $LiNbO_3:B$ [24], studies of crystals $LiNbO_3:B:Gd(1\text{ and }2)$ have not revealed optical deviations and effects twinning (Fig. 4). In the study of polar Z-cut plates, the mutually opposite crystallographic direction of domains of different signs makes it possible to obtain a fairly clear picture of the ferroelectric macrodomain structure during etching (Fig. 4, *a*, *b*). For crystals $LiNbO_3:B:Gd$ on plates cut perpendicular to the growth axis, the arrangement of nonperiodic concentric macrodomains of different signs (growth bands) with blurred domain boundaries is typical for lithium niobate crystals doped with rare earth elements (REE) (Fig. 4, *a*, *b*). Apparently, as for lithium niobate crystals doped with any other REE, the macrodomain structure of the Z-cut of crystals $LiNbO_3:B:Gd$ repeats the shape of the isotherm at the interface, and the specific location of the macrodomains (concentric growth bands) is determined by convection processes in the melt. The macrostructure of the central part of the plates is similar in both crystal samples $LiNbO_3:B:Gd$ and consists of a mixed domain structure with some signs of self-organization processes (Fig. 4, *c–f*).

The microstructure of the crystal samples $LiNbO_3:B:Gd(1\text{ and }2)$ has significant differences. Thus, no pronounced cellular substructure of the crystal was found in the crystal $LiNbO_3:B:Gd(1)$ (Fig. 4, *g*). At the same time, in the crystal $LiNbO_3:B:Gd(2)$, the substructure of the crystal is clearly visible with the possibility of calculating the average cell size (about $3.4\,\mu$m, Fig. 4, *h*). At the microlevel, the crystal structure $LiNbO_3:B:Gd(2)$ (Fig. 4, *h*) is more homogeneous and balanced compared to crystals $LiNbO_3:B:Gd(1)$ (Fig. 4, *g*) and $LiNbO_3:Gd(0.42\,\text{mol.}\%\ Gd_2O_3)$ (Fig. 3, *e*, *f*) — does not contain clusters of triangular microdomains observed at the micro level. The cells of the structure in the crystal $LiNbO_3:B:Gd(2)$ (Fig. 4, *h*) are on average rather ordered. The quantity, distribution, and size of „boron“ micropores (less than $1\,\mu$m) detected after etching the samples demonstrates a more balanced state for the crystal $LiNbO_3:B:Gd(2)$ (Fig. 4, *h*), than for the crystal $LiNbO_3:B:Gd(1)$ (Fig. 4, *g*).

At the same time, the crystal $LiNbO_3:B:Gd(2)$ contains meso-level defects manifested in the local formation of inhomogeneities with incoherent or semi-coherent boundaries (Fig. 5). Two types of defects were found: mesoblasts of microuniformities (Fig. 5, *a*) and pronounced „spotted“ heterogeneities (Fig. 5, *b*). Such types of mesodefects usually indicate the possibility of formation of a second-phase crystal in this region. No such meso-level defects were found in the crystal $LiNbO_3:B:Gd(1)$.

Thus, the macrostructure of the crystal samples $LiNbO_3:B:Gd(1\text{ and }2)$ are very similar. At the same time, there are significant differences at the micro and meso levels. The microstructure of the crystal $LiNbO_3:B:Gd(2)$ is more balanced than that of the crystal $LiNbO_3:B:Gd(1)$. At the same time, at the meso level of the crystal $LiNbO_3:B:Gd(2)$, there are clearly pronounced inhomogeneities that are absent in the crystal $LiNbO_3:B:Gd(1)$. The introduction of boron into the charge improved the

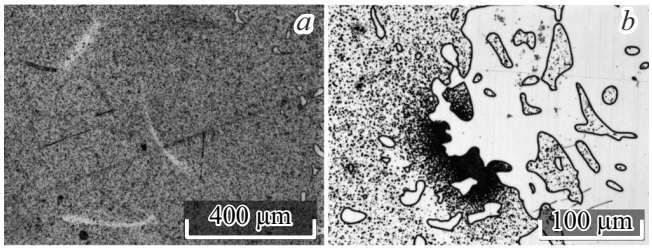

Figure 5. Meso-level defects in the crystal $LiNbO_3:B:Gd(2)$ before the HTEDA procedure.

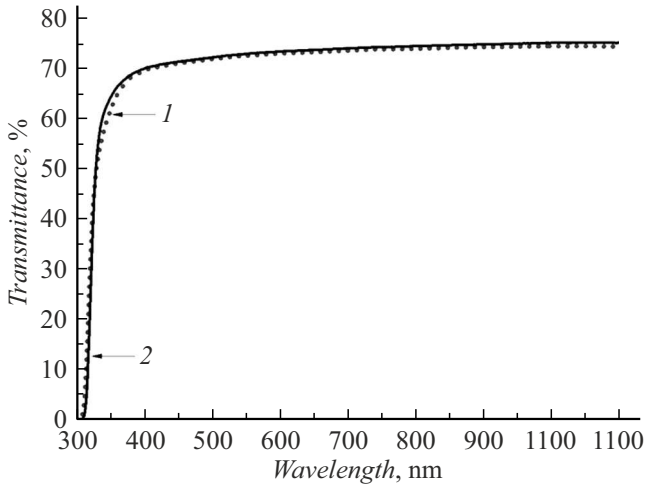

Figure 6. Crystal transmission spectra $LiNbO_3:Gd(0.42\,mol.\%\ Gd_2O_3)$ (*1*) and $LiNbO_3:B:Gd(1)$ (*2*). The thickness of the samples is ~ 1 mm.

macrostate of the crystals $LiNbO_3:B:Gd$, reducing the stress level compared to the crystal $LiNbO_3:Gd(0.42\,mol.\%\ Gd_2O_3)$, but the combined effect of the two impurities created conditions for the formation of a second phase with semicoherent boundaries, i.e., the appearance of chemical heterogeneity can transform into structural heterogeneity, creating a second phase.

Fig. 6 shows the transmission spectra of crystals $LiNbO_3:Gd(0.42\,mol.\%\ Gd_2O_3)$ and $LiNbO_3:B:Gd(1)$. A comparison of the above spectra shows a weak effect of boron impurity on the transmission coefficient, shape and position of the spectra. This is additionally confirmed by the calculated values of the crystal absorption edge $LiNbO_3:Gd(0.42\,mol.\%\ Gd_2O_3)$ and $LiNbO_3:B:Gd(1)$. The absorption edge of the crystal $LiNbO_3:Gd(0.42\,mol.\%\ Gd_2O_3)$ is ~ 310.0 nm, and the crystal $LiNbO_3:B:Gd(1)$ — ~ 311.3 nm. The transmission spectrum of $LiNbO_3:B:Gd(2)$ crystal is very close to the transmission spectrum of $LiNbO_3:B:Gd(1)$ crystal and is not shown in Fig. 6.

The analysis of the macro- and microstructure of crystals $LiNbO_3:B:Gd$ and their transmission spectra allows us to conclude that the joint doping of REE (Gd) and a nonmetallic element (B) makes it possible to obtain a single crystal with optical transmission parameters similar to the crystal $LiNbO_3:Gd$, and at the same time free from mechanical and structural stresses. It can be naturally assumed that a slight decrease in gadolinium concentration will improve the microstructure of the crystal $LiNbO_3:B:Gd$, eliminating the second phase precipitates (crystal $LiNbO_3:B:Gd(2)$ (Fig. 5).

The optical uniformity of the crystals $LiNbO_3:B:Gd(1$ and $2)$ was monitored by laser conoscopy. Conoscopic control of the optical properties of lithium niobate crystals is a clear and accessible research method, which is due to the relationship between the type, structure and properties of the conoscopic pattern with the structure, optical properties, orientation of the crystal, as well as the presence of mechanical stresses and various kinds of point and extended defects in it [38,39]. Conoscopic patterns obtained with low-power laser radiation (~ 1 mW), they reflect the state of crystal defects in the absence of the photorefraction effect, while conoscopic patterns recorded at high laser power (~ 90 mW) reflect both intrinsic and laser-induced crystal defects. Figure 7 shows the conoscopic patterns of crystals $LiNbO_3:B:Gd$ (1 and 2) after the HTEDA procedure, obtained by examining plates with a thickness of 3 mm.

The results of laser scanning along the plane of the entrance face of the studied crystals $LiNbO_3:B:Gd(1$ and $2)$ showed that both crystals are optically homogeneous. Fig. 7 shows two types of conoscopic patterns corresponding to both uniaxial crystals (1, 3, 5–8) and crystals with minor signs of abnormal biaxiality (2, 4). The conoscopic patterns (1, 3, 5–8) have circular symmetry where the integrity of the black „Maltese cross“ is maintained in the center of the field of vision, and he isochromes look like concentric circles with the center in the optical axis emergence point. It is this type of conoscopic patterns that indicates a relatively high optical uniformity of the samples and a good optical quality of the crystal. Conoscopic patterns (2, 4) contain insignificant signs of abnormal optical biaxiality when deformation occurs in the center of the black „Malthese cross“ in the form of displacement of the cross fragments (without separation) from the center in vertical direction corresponding to the optical indicatrix deformation direction of the crystal. Isochromes acquire a very weak ellipticity, while maintaining a regular geometric shape (Fig. 7 (2, 4)).

The conoscopic patterns of the studied crystals $LiNbO_3:B:Gd(1$ and $2)$ (Fig. 7) are similar to the conoscopic patterns of the pure $LiNbO_{3cong}$ crystal and are much less defective than the conoscopic patterns of the stoichiometric crystal composition ($LiNbO_{3stoich}$, $R = [Li]/[Nb] = 1$) [35]. The conoscopic patterns of the $LiNbO_{3stoich}$ crystal are significantly blurred at both 1 mW and 90 mW, and there are significant signs of abnormal optical biaxis and deformations of all branches of the Maltese cross, and the defects in the conoscopic patterns are significantly enhanced with increasing laser radiation power, which is associated with the presence of the photorefractive response of the $LiNbO_{3stoich}$ crystal [35]. Thus, in terms of optical uniformity, the crystals $LiNbO_3:B:Gd(1$ and $2)$ are close to the $LiNbO_{3cong}$ crystal and significantly exceed the $LiNbO_{3stoich}$ crystal.

It follows from Fig. 7 that the conoscopic patterns of crystal $LiNbO_3:B:Gd(2)$ are more perfect than the conoscopic patterns of crystal $LiNbO_3:B:Gd(1)$. This indicates a higher degree of optical uniformity of the double-doped crystal $LiNbO_3:B:Gd(2)$.

The appearance of areas of anomalous optical biaxis in conoscopic images is usually associated with the existence of local areas of optical inhomogeneity in a birefringent

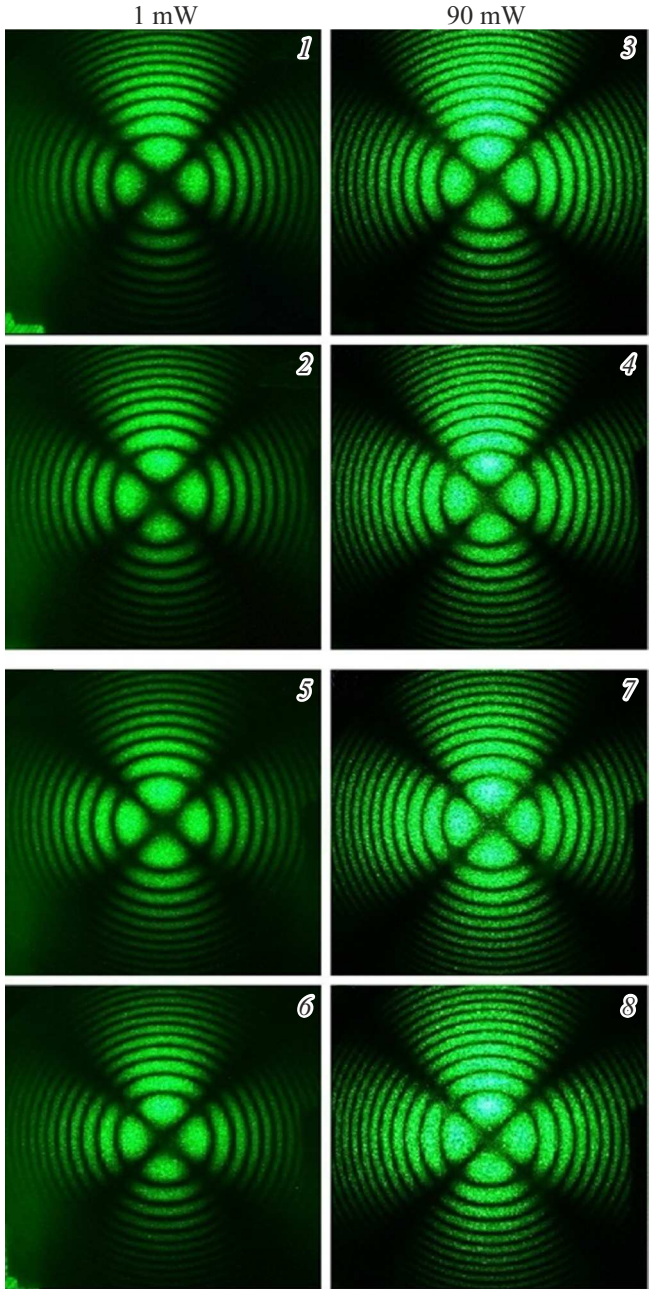

Figure 7. Conoscopic crystal patterns: *1–4* — $LiNbO_3:B:Gd(1)$, *5–8* — $LiNbO_3:B:Gd(2)$ after the HTEDA procedure, obtained by scanning along the plane of the input face with laser radiation with a power of 1 mW (*1, 2, 5, 6*) and 90 mW (*3, 4, 7, 8*). The thickness of the plates is 3 mm. The Z axis is perpendicular to the drawing plane. $\lambda = 532$ nm.

crystal. For doped lithium niobate crystals, this may be due to the segregation of impurities in the crystal, especially at significant concentrations of dopant cations. In accordance with the results of optical microscopy (Fig. 4, 5) obtained on crystal samples $LiNbO_3:B:Gd$ before the HTEDA procedure, it was expected that conoscopic analysis would show a higher degree of optical uniformity of the crystal $LiNbO_3:B:Gd(1)$, since the crystal $LiNbO_3:B:Gd(2)$ contains meso-level defects that manifest themselves in the formation of inhomogeneities with incoherent or semi-coherent boundaries. Such types of mesodefects suggest the possibility of forming a second-phase crystal in this region, which leads to a change in the elastic characteristics of the crystal and the appearance of mechanical stresses that locally distort the optical indicatrix of the optically uniaxial crystal [35]. However, the laser conoscopy method has shown that the crystal $LiNbO_3:B:Gd(2)$ has a higher degree of optical uniformity. This may be a consequence of the redistribution of defects as a result of the HTEDA.

Structural rearrangements and phase transitions in crystals can be detected using thermal analysis. Fig. 8 shows the curves of differential scanning calorimetry (DSC) of crystals $LiNbO_3:B:Gd$(1 and 2). The heating curves show a thermal effect in the temperature range of $T = 720\,^{\circ}\mathrm{C}-760\,^{\circ}\mathrm{C}$, the temperature of which depends on the concentration of the dopant. The type of this thermal effect is similar to the glass transition process. This effect can be explained by the presence of a boron dopant, which is a glass-forming component and a strong complexing agent. This is confirmed by the study in Ref. [40], which investigated glasses based on lithium niobate crystal and boron oxide, as well as lithium-niobium-boron glass. In this study, the DSC method revealed a similar thermal effect in the close temperature range [40]. Our study showed that a decrease in the boron content in the crystal $LiNbO_3:B:Gd(2)$ (Table 2) leads to a decrease in the glass transition temperature from $T_g = 760\,^{\circ}\mathrm{C}$ in the crystal $LiNbO_3:B:Gd(1)$ to $T_g = 728\,^{\circ}\mathrm{C}$ (Fig. 8).

In the temperature range of $T = 1210\,^{\circ}\mathrm{C}-1213\,^{\circ}\mathrm{C}$, an inflection is detected due to a ferroelectric phase transition (FPT) of the second kind in crystals $LiNbO_3:B:Gd$(1 and 2) (Fig. 8). A method for determining the Curie temperature in lithium niobate crystals from thermal analysis curves is presented in Ref. [26]. For crystals $LiNbO_3:B$, the FPT is observed at a lower temperature and, accordingly, T_C is $\sim 1189\,^{\circ}\mathrm{C}-1190\,^{\circ}\mathrm{C}$ [24], which is noticeably less than for crystals $LiNbO_3:B:Gd$(1 and 2) (Fig. 8).

As is known, T_C can change with changes in the stoichiometry of the lithium niobate crystal, as well as the type and concentration of the dopant [9,23,26]. Thus, T_C of double-doped crystals $LiNbO_3:B:Gd$(1 and 2) is $\sim 1210\,^{\circ}\mathrm{C}-1213\,^{\circ}\mathrm{C}$ (Fig. 8), $T_C \sim 1189\,^{\circ}\mathrm{C}-1190\,^{\circ}\mathrm{C}$ for single-doped crystals $LiNbO_3:B$ [24] and $T_C \sim 1135\,^{\circ}\mathrm{C}$ for crystal $LiNbO_3:Gd$ [23]. At the same time, T_C of the crystal of $LiNbO_{3cong}$ is $\sim 1145\,^{\circ}\mathrm{C}$ [24]. Thus, here we do not observe the additive effect of the impurity on T_C, similar to the additive effect of tantalum and magnesium impurities on T_C crystals $LiNbO_3:Ta:Mg$ [26]. Despite the fact that trivalent impurities like Gd^{3+} are predominantly embedded in lithium octahedra O_6 of the ideal crystal structure $LiNbO_3$ [41], reducing the content of point defects Nb_{Li}, the gadolinium impurity, like the impurities of other REE, reduces the Curie temperature [23]. In turn, the presence of boron in the melt makes it possible to radically

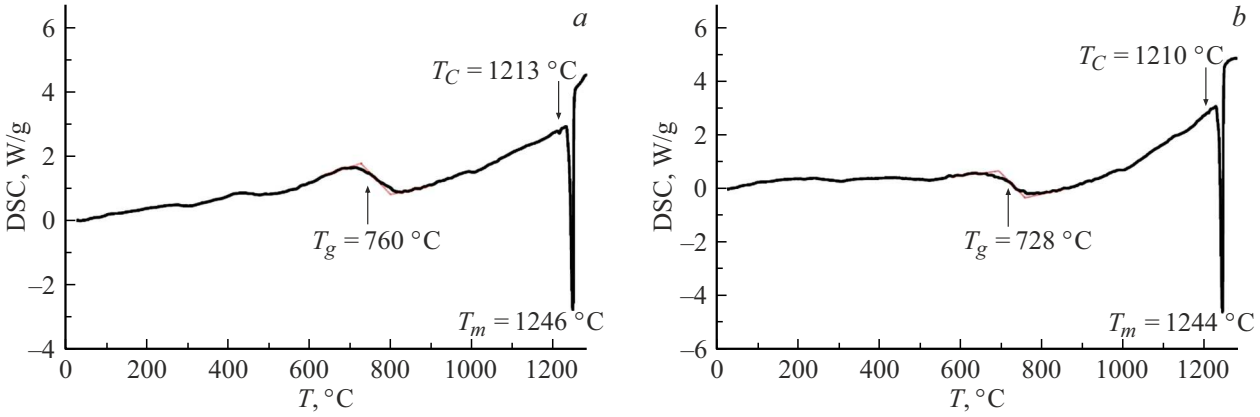

Figure 8. DSC curves of crystals: *a* — $LiNbO_3:B:Gd(1)$, *b* — $LiNbO_3:B:Gd(2)$.

reduce the content of Nb_{Li} defects in $LiNbO_3$ crystals and bring the crystal composition closer to the stoichiometric one ($R = 1$) by binding excess niobium in a melt of congruent composition into strong complexes that do not they participate in the crystallization process [24]. Thus, the combination of the type and concentration of dopants (B and Gd) chosen in this work led to the formation of such ionic complexes in a melt of congruent composition, which, to a greater extent than when using a melt containing only boron, brought the composition of the lithium niobate crystal closer to stoichiometric, i.e. in this case, a synergistic effect is observed. The effect of impurities, which opens up new opportunities in the development of technologies for the synthesis of functional materials based on lithium niobate with specified characteristics.

The high-intensity endothermic effect (Fig. 8) is associated with the melting of crystals $LiNbO_3:B:Gd$(1 and 2) and is detected at a temperature of $T_m = 1244\,^\circ\text{C} - 1246\,^\circ\text{C}$. The difference in the concentration of the dopant additive (Tables 1, 2) has practically no effect on the melting point of crystals of $LiNbO_3:B:Gd$(1 and 2) (Fig. 8). In this case, the melting point of the crystals of $LiNbO_3:B$ is $\sim 1262\,^\circ\text{C} - 1264\,^\circ\text{C}$, and the melting point of crystal of $LiNbO_{3cong}$ is $\sim 1257\,^\circ\text{C}$ [24]. The decrease in the melting point of crystals $LiNbO_3:B:Gd$(1 and 2) is probably caused by a significant change in the physico-chemical characteristics of the melt of the system Li_2O-Nb_2O_5-Gd_2O_3-B_2O_3 during the formation of boron and gadolinium-containing ion complexes.

The crystal $LiNbO_3$, as a nonstoichiometric phase of variable composition, has a fairly high degree of defect [4,14,24]. Intrinsic and impurity defects play a significant role in the formation of the physical properties of lithium niobate crystal [42]. In this regard, it is necessary to study the properties of $LiNbO_3$ crystals in close relationship with the features of their defective structure. Niobium cations are partially embedded in the larger lithium octahedron O_6 during growing of a Li-deficient crystal of $LiNbO_{3cong}$, resulting in the formation of deep electron traps in the crystal structure — point defects Nb_{Li}^{4+}. Vacancies in lithium positions are formed in the crystal to preserve electroneutrality (V_{Li}^-). According to the split model of Li vacancies, the cationic sublattice of the crystal of $LiNbO_{3cong}$ contains ~ 1 mol.% of point defects Nb_{Li}^{4+} and ~ 4 mol.% of point defects V_{Li}^- [43,44]. A negatively charged lithium vacancy attracts a positively charged hydrogen ion, which is bound to an oxygen ion in the crystal structure by a hydrogen bond [45,46]. As a result, a complex defect forms in the crystal structure (V_{Li}-OH). Similarly, complex defects Nb_{Li}-OH, Gd_{Li}-OH and others form in the crystal structure $LiNbO_3$, affecting the transformation and generation of laser radiation by the crystal, thermal fixation of holograms, photoluminescence, photorefraction effect, and crystal conductivity [4,45,46].

The concentration of hydroxyl groups in a lithium niobate crystal associated with various defects in the crystal structure can be determined using IR absorption spectroscopy in the region of valence vibrations of OH groups. The complex defect (V_{Li}-OH) in the IR absorption spectra corresponds to bands with frequencies 3467, 3480 and 3489 cm^{-1} and a half-width of about $\sim 30\,cm^{-1}$. The number of intrinsic defects Nb_{Li} in crystals $LiNbO_3$ decreases with an increase in the value of R, which can be increased, including by introducing dopant additives into the crystal structure [24]. Moreover, the presence of boron dopant admixture in the congruent melt makes it possible to significantly reduce the number of point defects Nb_{Li}^{4+} [24].

Fig. 9 shows the IR absorption spectra in the region of valence vibrations of OH groups of double-doped crystals of $LiNbO_3:B:Gd$(1 and 2), as well as the crystal of $LiNbO_{3cong}$, selected in this study, as an object of comparison. The main parameters of the spectral lines, as well as the concentration of hydroxyl groups in the studied crystals, are presented in Table 3. The number of absorption lines in the IR spectra is the same, which indicates an equal number of unequal positions of hydrogen atoms in the structure of the studied lithium niobate crystals (Table 3). Fig. 9 and Table 3 show that the IR absorption

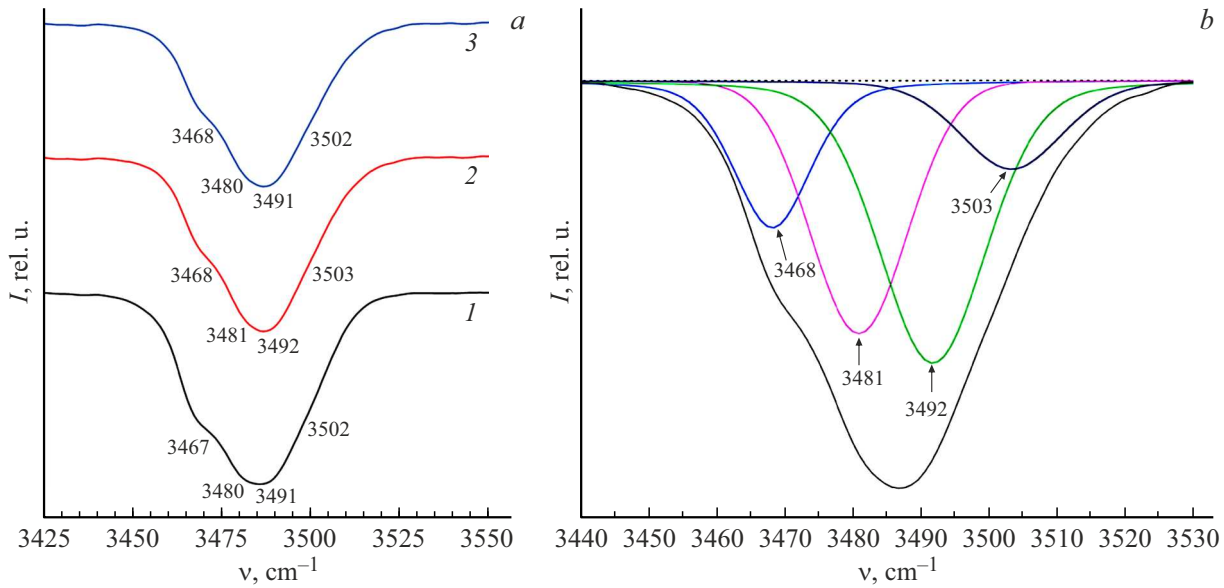

Figure 9. IR absorption spectra in the region of valence vibrations of OH groups (*a*) of $LiNbO_{3cong}$ crystals — *1*, $LiNbO_3:B:Gd(1)$ — *2*, $LiNbO_3:B:Gd(2)$ — *3* and band decomposition (*b*) of the IR absorption spectrum crystal $LiNbO_3:B:Gd(1)$ into components.

spectra of $LiNbO_3:B:Gd$(1 and 2) crystals show some differences compared to the IR spectrum of the crystal of $LiNbO_{3cong}$, changes in the intensity and half-width of the absorption line components. The data obtained indicate a change in the state of the defective structure of crystals $LiNbO_3:B:Gd$(1 and 2) due to the presence of OH hydroxyl groups and the synergistic effect of co-alloying a congruent lithium niobate melt with boron and gadolinium. In particular, the value of R of double-doped crystal is close to unity.

Doping of the crystal $LiNbO_3$ with cations Gd^{3+}, in turn, leads to a change in the lengths of bonds ⟨Gd-O⟩, ⟨Oh-O⟩ and to distortion of oxygen-octahedral clusters of MeO_6 (Me-Li, Nb, impurity metal), responsible for the nonlinear optical and ferroelectric properties of the crystal [45,46]. These effects lead to a disordering of the crystal structure and are manifested in an increase in the half-width of some absorption lines in the IR spectra of $LiNbO_3:B:Gd$ crystals relative to the spectrum of $LiNbO_{3cong}$ the crystal (Fig. 9, Table. 3).

Based on the IR absorption spectra, we calculated the volume concentration of OH groups in the studied crystals of different compositions using the Klauer method [34]. The concentration of OH groups in double-doped crystals of $LiNbO_3:B:Gd$(1 and 2) is significantly higher than in the $LiNbO_{3cong}$ crystal (Table 3). Potentially, Gd^{3+} cations can occupy one of three possible positions in the crystal structure $LiNbO_3$: the main octahedral positions of lithium and niobium, or be embedded in vacant octahedra [47]. The location of the cation Gd^{3+} in a relatively small free octahedron is unlikely due to its larger ionic radius ~ 0.94 Å [48]. At the same time, it is known that dopant metal cations at relatively low concentrations are preferably embedded in the main octahedral positions of lithium because the lithium octahedron has a larger size than niobium octahedron [4,49]. However, a small amount of dopant REE in a certain concentration range can also be localized in the niobium octahedron of the crystal structure [50]. When the point defect Nb_{Li} is displaced by the ion Gd^{3+}, the excess positive charge of Gd^{2+}_{Li} is compensated by two negative point defects V^-_{Li}. Each structural defect Nb^{4+}_{Li} is compensated by four point defects V^-_{Li} to preserve electroneutrality in $LiNbO_{3cong}$ crystal [4]. Thus, the number of defect centers V^-_{Li}, which can attract a hydrogen atom and form a complex defect (V_{Li}-OH), in $LiNbO_3:B:Gd$ crystals should be less than in $LiNbO_{3cong}$ crystal (Table 3). It was found in Ref. [24] that the concentration of OH hydroxyl groups in $LiNbO_3:B$ crystals of different compositions depends on the concentration of boron oxide in the charge from which the boron-containing crystals were grown, and varies from $3.4 \cdot 10^{17}$ up to $6.4 \cdot 10^{17}$ cm^{-3}, i.e. It is either close to or almost twice the concentration of hydroxyl groups in the $LiNbO_{3cong}$ crystal. In this case, $LiNbO_3:B$ crystals have a value of $R \approx 1$ and a significantly lower concentration of point structural defects Nb_{Li} and V_{Li} compared with $LiNbO_{3cong}$ crystal [24]. Thus, the increase in the concentration of hydroxyl groups in $LiNbO_3:B:Gd$(1 and 2) crystals is apparently due not to structural, but to physico-chemical and technological factors. Indeed, solid-phase synthesis of a charge for growing $LiNbO_3:B:Gd$ crystals occurs from a mixture of oxides and boric acid: Nb_2O_5-Li_2O-Gd_2O_3-H_3BO_3, i.e., a hydrogen-containing component is used in the synthesis of the charge, which determines an increase in the concentration of OH groups in the crystal (Table. 3).

The resistance of $LiNbO_3:B:Gd$(1 and 2) crystals to damage by laser radiation was studied by the PILS method.

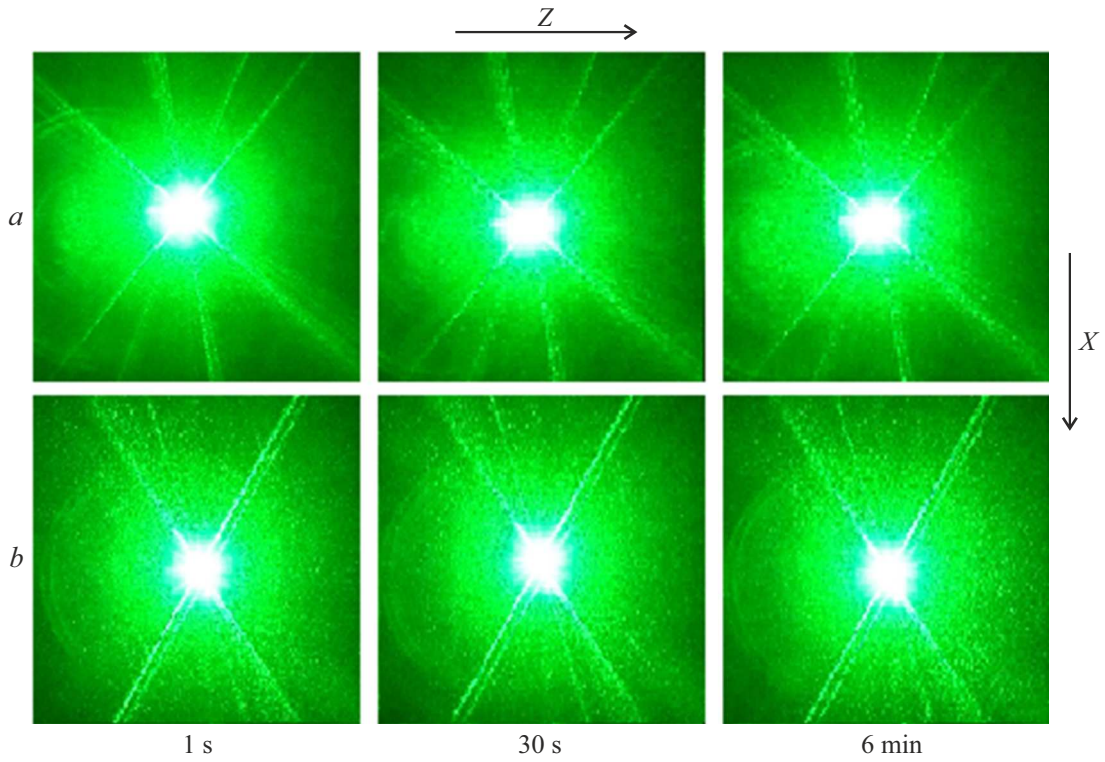

Figure 10. PILS patterns of crystals: $LiNbO_3:B:Gd(1)$ — *a*, $LiNbO_3:B:Gd(2)$ — *b*. $\lambda = 532$ nm. $P = 6.3$ W/cm^2.

Table 3. Values of frequencies (ν, cm^{-1}), widths (S, cm^{-1}) and intensities (I, rel. u.) lines in the IR absorption spectra, concentrations of OH groups (C(OH)/cm^3) in $LiNbO_{3cong}$ crystal and double-doped crystals of $LiNbO_3:B:Gd$(1 and 2) at $t = 25\,^\circ$C

Crystals	ν	I	S	C(OH)/cm^3
$LiNbO_{3cong}$	3467	12.18	14.00	$3.26 \cdot 10^{17}$
	3480	16.54	16.95	
	3491	17.75	17.94	
	3502	5.96	14.40	
$LiNbO_3:B:Gd(1)$	3468	8.33	13.42	$4.36 \cdot 10^{17}$
	3481	14.21	16.80	
	3492	15.80	18.44	
	3503	4.96	17.69	
$LiNbO_3:B:Gd(2)$	3468	7.94	13.22	$4.05 \cdot 10^{17}$
	3480	13.44	15.93	
	3491	14.64	16.92	
	3502	6.56	17.72	1

Fig. 10 shows the time dependences of the PILS patterns of $LiNbO_3:B:Gd$(1 and 2) crystals. Fig. 10 shows that only circular scattering by static structural defects is observed for the studied crystals, even after irradiation for 6 min with laser radiation ($p = 6.3$ W/cm^2), while the speckle structure of the PILS indicatrix does not opens. A similar PILS pattern is observed in $LiNbO_{3cong}$ crystal [35]. Since the disclosure of the speckle structure of PILS is a consequence of the photorefraction effect, it can be concluded that there is no photorefraction effect in $LiNbO_3:B:Gd$(1 and 2) crystals at the laser radiation intensity used by us. For comparison, the PILS of $LiNbO_{3stoich}$ crystal [35] significantly differs from the PILS of the crystals of $LiNbO_{3cong}$ [35] and $LiNbO_3:B:Gd$(1 and 2), Fig. 10: during the first 30 s the scattering pattern of the $LiNbO_{3stoich}$ crystal [35] transforms from a rounded shape into an oval elongated along the polar axis of the crystal after 240 s in the stationary state, the shape of the speckle structure PILS of the $LiNbO_{3stoich}$ crystal has the form of an asymmetric figure of eight relative to the normal to the main section of the crystal, due to a change in the refractive index, the scattering angle is 56°. $LiNbO_{3stoich}$ crystal is distinguished by a highly ordered cationic sublattice, however, it has an inhomogeneous refractive index along the polar axis, a high concentration of defects with electrons localized on them, and a much greater photorefraction and PILS effect than crystals of $LiNbO_{3cong}$ [35] and $LiNbO_3:B:Gd$(1 and 2) (Fig. 10), which can significantly reduce the efficiency of nonlinear optical transformations. Thus, the combination of two non-photorefractive impurities of different chemical nature with the proposed ratio of their concentrations and the used technological growth parameters leads to the production

of nonlinear optical crystals of $LiNbO_3:B:Gd$ with high optical uniformity and resistance to optical damage.

Conclusion

A granular monophase charge of $LiNbO_3:B:Gd$ was synthesized from a mixture of extremely pure components $Li_2CO_3:Nb_2O_5:Gd_2O_3:H_3BO_3$. Chokhralsky method was used to obtain double-doped crystals

$LiNbO_3:(0.58\cdot10^{-3}\ B_2O_3):(0.51\,\text{mol.\%}\ Gd_2O_3)$ and

$LiNbO_3:(0.32\cdot10^{-3}\ B_2O_3):(0.53\,\text{mol.\%}\ Gd_2O_3)$–

$LiNbO_3:B:Gd(1)$ and $LiNbO_3:B:Gd(2)$,

from the melt which are characterized by high compositional uniformity along the growth axis and high optical quality. A decrease in the boron concentration in the melt was found during the production of single crystals of $LiNbO_3:B:Gd(1$ and $2)$ at an initial boron concentration in the charge of 0.03 mol.% of B_2O_3 almost tripled, which is due to the evaporation of boron during melt preparation and crystal growth.

The macro- and microstructure of crystals of $LiNbO_3$:B:Gd(1 and 2) has been studied by optical microscopy before HTEDA and it has been compared with the macro- and microstructure of the crystal of $LiNbO_3:Gd(0.42\,\text{mol.\%}\ Gd_2O_3)$. This allowed evaluating the effect of the chemical composition of crystals on the configuration of the growth defect structure of crystals $LiNbO_3:B:Gd(1$ and $2)$. The macrostructure of the samples of $LiNbO_3:B:Gd(1$ and $2)$ crystal is very similar. At the same time, there are some differences at the micro and meso levels. Thus, $LiNbO_3:B:Gd(1)$ crystal has almost no cellular substructure, unlike $LiNbO_3:B:Gd(2)$ crystal. The number, distribution, and size of „boron" micropores demonstrate a more balanced state for $LiNbO_3:B:Gd(2)$ crystal than for $LiNbO_3:B:Gd(1)$ crystal. $LiNbO_3:B:Gd(2)$ crystal contains pronounced meso-level inhomogeneities that are not present in $LiNbO_3:B:Gd(1)$ crystal. The patterns of formation of the macro- and microdomain structures of as-grown $LiNbO_3:B:Gd$ crystals provide significant additional information about the physico-chemical characteristics of the crystal-melt system and the mechanisms of crystallization.

Comparison of transmission spectra of crystals of $LiNbO_3:Gd(0.42\,\text{mol.\%}\ Gd_2O_3)$, $LiNbO_3:B:Gd(1)$ and $LiNbO_3:B:Gd(2)$ showed a weak effect of boron impurity on the transmission coefficient and the appearance of the spectra as a whole. Analysis of the macro- and microstructure of crystals of $LiNbO_3:B:Gd(1)$, $LiNbO_3:B:Gd(2)$ and $LiNbO_3:Gd(0.42\,\text{mol.\%}\ Gd_2O_3)$, as well as their transmission spectra, indicates that co-doping with REE (Gd) and a nonmetallic element (B) makes it possible to obtain single crystals of $LiNbO_3:B:Gd$ with optical transmission parameters similar to $LiNbO_3:Gd$ crystal, but free from mechanical and structural stresses.

The applied HTEDA technological modes require adjustments due to the insufficiently high degree of single-domain state of $LiNbO_3:B:Gd(1$ and $2)$ crystals. The results of the examination of plates of $LiNbO_3:B:Gd(1$ and $2)$ crystals after HTEDA by laser conoscopy showed their high optical uniformity. At the same time, $LiNbO_3:B:Gd(2)$ crystal has a higher optical uniformity, which may be a consequence of the redistribution of defects as a result of the HTEDA.

$LiNbO_3:B:Gd(1$ and $2)$ crystals have a very high Curie temperature ($T_C\sim1210\,^\circ\text{C}-1213\,^\circ\text{C}$) in comparison with crystals of $LiNbO_{3cong}$ ($T_C\sim1142\,^\circ\text{C}$), $LiNbO_3:Gd$ ($T_C\sim1135\,^\circ\text{C}$) and $LiNbO_3:B$ ($T_C\sim1189\,^\circ\text{C}-1190\,^\circ\text{C}$). It was found that the combination of the type and concentration of dopants (B and Gd) led to the formation of such ionic complexes in a melt of congruent composition, which, to a greater extent than when using a melt containing only one boron, brought the composition of the lithium niobate crystal closer to the stoichiometric one. In this case, there is an increase in T_C, which indicates the ordering of the crystal structure. In other words, a synergistic effect of the influence of impurities has been discovered, which opens up new opportunities in the development of technologies for the synthesis of functional materials with specified characteristics based on lithium niobate crystals. A slight decrease in the melting point of $LiNbO_3:B:Gd(1$ and $2)$ crystals compared to $LiNbO_3:B$ and $LiNbO_{3cong}$ crystals is likely attributable to a significant change in the physico-chemical characteristics of the melt of the system of Li_2O-Nb_2O_5-Gd_2O_3-B_2O_3 during the formation of ionic complexes containing boron and gadolinium.

IR absorption spectroscopy in $LiNbO_3:B:Gd(1$ and $2)$ crystals did not reveal a decrease in the number of absorption bands corresponding to valence vibrations of hydrogen atoms of hydroxyl groups. There is a change in the intensity parameter and the half-width of the components of the absorption bands of $LiNbO_3:B:Gd(1$ and $2)$ crystals compared with $LiNbO_{3cong}$, which indicates a change in the state of the defective structure of double-doped crystals. It is shown that the increase in the concentration of hydroxyl groups in $LiNbO_3:B:Gd(1$ and $2)$ crystals is attributable to physico-chemical and technological factors.

According to PILS data, $LiNbO_3:B:Gd(1$ and $2)$ crystals are highly resistant to optical damage. In PILS patterns, only circular scattering of the laser beam on static structural defects is observed, while the speckle structure of the PILS indicatrix is not revealed during the entire experiment at the involved laser power density ($6.3\,\text{W/cm}^2$). That is, there is no photorefraction effect in $LiNbO_3:B:Gd(1$ and $2)$ crystals with a laser power density of $\leq 6.3\,\text{W/cm}^2$.

Thus, the double doping of a congruent lithium niobate single crystal with non-photorefractive impurities (B and Gd) of various chemical nature proposed in the work and correctly selected technological parameters for growing single crystals made it possible to obtain optically highly perfect and compositionally homogeneous single crystals of $LiNbO_3:(0.58\cdot10^{-3}\ B_2O_3):(0.51\,\text{mol.\%}\ Gd_2O_3)$ and $LiNbO_3:(0.32\cdot10^{-3}\ B_2O_3):(0.53\ \text{mol.\%}\ Gd_2O_3)$, which

may be promising for the development of functional elements for laser radiation conversion.

Funding

The work was carried out with the support of the Ministry of Science and Higher Education of the Russian Federation, the registration number of the scientific topic is FMEZ-2025-0055.

Conflict of interest

The authors declare that they have no conflict of interest.

References

[1] C. Guanyu, L. Nanxi, D.N. Jun, L. Hong-Lin, Z. Yanyan, H.F. Yuan, Y.T.L. Lennon, Y. Yu, L. Ai-Qun, J.D. Aaron. Adv. Photonics, **4** (3), 034003 (2022). DOI: 10.1117/1.AP.4.3.034003
[2] R.S. Weis, T.K. Gaylord. Appl. Phys. A, **37**, 191 (1985). DOI: 10.1007/BF00614817
[3] Y. Guo, L. Liu, D. Liu, S. Deng, Y. Zhi. Appl. Opt., **44** (33), 7106 (2005). DOI: 10.1364/ao.44.007106
[4] N.V. Sidorov, T.R. Volk, B.N. Mavrin, V.T. Kalinnikov. *Niobat litiya: defekty, fotorefraktsiya, kolebatelny spektr, polyaritony* (Nauka, M., 2003) (in Russian).
[5] Y. Wang, R. Wang, J. Yuan, Y. Wang. J. Lumin., **147**, 242 (2014). DOI: 10.1016/j.jlumin.2013.11.032
[6] M. Carrascosa, A. García-Cabañes, M. Jubera, J.B. Ramiro, F. Agulló-López. Appl. Phys. Rev., **2** (4), 040605 (2015). DOI: 10.1063/1.4929374
[7] K.M. Mambetova, S.M. Shandarov, A.I. Tatyannikov, S.V. Smirnov. Russ. Phys. J., **62** (4), 658 (2019). DOI: 10.1007/s11182-019-01760-6
[8] K. Chen, Y. Zhu, Z. Liu, D. Xue. Molecules, **26** (22), 7044 (2021). DOI: 10.3390/molecules26227044
[9] H.M. O'Bryan, P.K. Gallagher, C.D. Brandle. J. Am. Ceram. Soc., **68** (9), 493 (1985). DOI: 10.1111/J.1151-2916.1985.TB15816.X
[10] Yu.S. Kuz'minov. *Elektroopticheskii i nelineinoopticheskii kristall niobata litiya* (Nauka, M., 1987) (in Russian).
[11] D. Xue, K. Kitamura, J. Wang. Opt. Mater., **23**, 399 (2003). DOI: 10.1016/S0925-3467(02)00326-9
[12] H.D. Megaw. Acta Cryst., **7** (2), 187 (1954). DOI: 10.1107/s0365110x54000527
[13] M.N. Palatnikov, N.V. Sidorov, O.V. Makarova, D.V. Manukovskaya, L.A. Aleshina, A.V. Kadetova. J. Am. Ceram. Soc., **100** (8), 3703 (2017). DOI: 10.1111/jace.14851
[14] T. Volk, M. Wohlecke. *Lithium Niobate. Defects, Photorefraction and Ferroelectric Switching* (Springer, Berlin, 2008)
[15] A. Kling, J.G. Marques. Crystals., **11** (5), 501 (2021). DOI: 10.3390/cryst11050501
[16] M.N. Palatnikov, N.V. Sidorov, A.Yu. Pyatyshev, P.P. Sverbil, N.A. Teplyakova, O.V. Makarova. Opt. Mater., **135**, 113241 (2023). DOI: 10.1016/j.optmat.2022.113241
[17] O. Sánchez-Dena, S.D. Villalobos-Mendoza, R. Farías, C.D. Fierro-Ruiz. Crystals., **10** (11), 990 (2020). DOI: 10.3390/cryst10110990
[18] C. Cochard, M. Guennou, T. Spielmann, N.V. Hoof, A. Halpin, T.J. Granzow. Appl. Phys., **123** (15), 154105 (2018). DOI: 10.1063/1.5021758
[19] Y. Kong, F. Bo, W. Wang, D. Zheng, H. Liu, G. Zhang, R. Rupp, J. Xu. Adv. Mater., **32** (3), 1806452 (2019). DOI: 10.1002/adma.201806452
[20] T.S. Chernaya, T.R. Volk, I.A. Verin, V.I. Simonov. Crystallogr. Rep., **53** (4), 573 (2008). DOI: 10.1134/S106377450804007X
[21] T.S. Chernaya, B.A. Maksimov, T.R. Volk, N.M. Rubinina, V.I. Simonov. JETPL, **73** (2), 103 (2001). DOI: 10.1134/1.1358430
[22] M.N. Palatnikov, O.V. Makarova, N.V. Sidorov. *Rostovye i tekhnologicheskie defekty kristallov niobata litiya razlichnogo khimicheskogo sostava: atlas,* Izd-vo FITs KNTs RAN, Apatity, 2018 (in Russian).
[23] M.N. Palatnikov, I.V. Biryukova, N.V. Sidorov, A.V. Denisov, V.T. Kalinnikov, P.G.R. Smith, V.Ya. Shur. J. Cryst. Growth., **291** (2), 390 (2006). DOI: 10.1016/J.JCRYSGRO.2006.03.022
[24] N.V. Sidorov, M.N. Palatnikov, N.A. Tepliakova, I.V. Biryukova, R.A. Titov, O.V. Makarova, S.M. Masloboeva. *Monokristally niobata i tantalata litiya raznogo sostava i genezisa* (Izd-vo RAN, M., 2022) (in Russian).
[25] M. Palatnikov, N. Sidorov, A. Kadetova. O. Makarova. Opt. Mater., **122** (A), 111755 (2021). DOI: 10.1016/j.optmat.2021.111755
[26] M.N. Palatnikov, N.V. Sidorov, V.I. Skiba, D.V. Makarov, I.V. Biryukova, Y.A. Serebryakov, O.E. Kravchenko, Y.I. Balabanov, V.T. Kalinnikov. Inorg. Mater., **36** (5), 489 (2000). DOI: 10.1007/BF02758054
[27] K. Raksanyc, A. Peter, Z. Szaller, I. Forizs, S. Erdei. Acta Phys. Hung., **61** (2), 213 (1987). DOI: 10.1007/BF03155894
[28] M. Palatnikov, O. Makarova, A. Kadetova, N. Sidorov, N. Teplyakova, I. Biryukova, O. Tokko. Materials, **16** (13), 4541 (2023). DOI: 10.3390/ma16134541
[29] X.H. Zhen, H.T. Li, Z.J. Sun, S.J. Ye, L.C. Zhao, Y.H. Xu. Mater. Lett., **58** (6), 1000 (2004). DOI: 10.1016/j.matlet.2003.08.005
[30] T. Bodziony, S.M. Kaczmarek, J. Hanuza. J. Alloys Compd., **451** (1–2), 240 (2008). DOI: 10.1016/j.jallcom.2007.04.189
[31] G. Xu, J. Zhu, B. Xiao, X. Yang, X. Wang. Cryst. Res. Technol., **31** (2), K20 (1996). DOI: 10.1002/crat.2170310226
[32] X. Yang, G. Xu, H. Li, J. Zhu, X. Wang. Cryst. Res. Technol., **31** (4), 521 (1996). DOI: 10.1002/crat.2170310418
[33] K. Kasemir, K. Betzler, B. Matzas, B. Tiegel, T. Wahlbrink, M. Wöhlecke, B. Gather, N. Rubinina, T. Volk. J. Appl. Phys., **84** (9), 5191 (1998). DOI: 10.1063/1.368769
[34] S. Klauer, M. Wḧlecke, S. Kapphan. Phys. Rev. B., **45** (6), 2786 (1992). DOI: 10.1103/PhysRevB.45.2786
[35] N.V. Sidorov, O.Yu. Pikul', N.A. Teplyakova, M.N. Palatnikov. *Lazernaya konoskopiya i fotoindutsirovannoe rasseyanie sveta v issledovaniyakh svoystv nelineyno-opticheskogo monokristalla niobata litiya* (RAN, M., 2019) (in Russian).
[36] Yu.M. Tairov, V.P. Tsvetkov. *Technology of semiconductor and dielectric materials* (Higher School, Moscow, 1983) (in Russian).
[37] H. Can, W. Shichao, Y. Ning. J. Alloys Compd., **502** (1), 211 (2010). DOI: 10.1016/J.JALLCOM.2010.04.146
[38] K.A. Rudoĭ, V.I. Stroganov, L.V. Alekseeva, B.V. Nabatov, A.F. Konstantinova, E.A. Evdishchenko, B.I. Kidyarov. Crystallogr. Rep., **48** (2), 300 (2003). DOI: 10.1134/1.1564211

[39] O.Y. Pikoul. J. Appl. Crystallogr., **43** (5/1), 955 (2010). DOI: 10.1107/S0021889810022375
[40] E. Muzi, M. Cavillon, M. Lancry, F. Brisset, R. Que, D. Pugliese, D. Janner, B. Poumellec. Crystals, **11** (3), 290 (2021). DOI: 10.3390/cryst11030290
[41] C. Koyama, J. Nozawa, K. Maeda, K. Fujiwara, S. Uda. J. Appl. Phys., **117** (1), 014102 (2015). DOI: 10.1063/1.4905286
[42] C.-T. Chia, C.-C. Lee, P.-J. Chang, M.-L. Hu, L.J. Hu. Appl. Phys. Lett., **86** (18), 182901 (2005). DOI: 10.1063/1.1922083
[43] N. Lyi, K. Kitamura, F. Izumi, J.K. Yamamoto, T. Hayashi, H. Asano, S. Kimura. J. Solid State Chem., **101** (2), 340 (1992). DOI: 10.1016/0022-4596(92)90189-3
[44] P. Lerner, C. Legras, J.P. Dumas. J. Cryst. Growth., 3−4, 231 (1968). DOI: 10.1016/0022-0248(68)90139-5
[45] J.M. Cabrera, J. Olivares, M. Carrascosa, J. Rams, R. Müller, E. Dieguez. Adv. Phys., **45** (5), 349 (1996). DOI: 10.1080/00018739600101517
[46] K. Lengyel, A. Peter, L. Kovacs, G. Corradi, L. Palfalvi, J. Hebling, M. Unferdorben, G. Dravecz, I. Hajdara, Z. Szaller, K. Polgar. Appl. Phys. Rev., **2** (4), 040601 (2015). DOI: 10.1063/1.4929917
[47] L. Kovács, L. Rebouta, J.C. Soarest, M.D. Silva, M. Hage-ali, J. Stoquert, P. Siffert, J.A. Sanz-Garcia, G. Corradi, Z. Szaller, K. Polgár. J. Phys.: Condens. Matter., **5**, 781 (1993). DOI: 10.1088/0953-8984/5/7/006
[48] R.D. Shannon. Acta Crystallographica, A **32**, 751 (1976). DOI: 10.1107/s0567739476001551
[49] L. Kovács, Z. Szaller, K. Lengyel, G. Corradi. Opt. Mater., **37**, 55 (2014). DOI: 10.1016/j.optmat.2014.04.043
[50] L. Kovács, L. Kocsor, Z. Szaller, I. Hajdara, G. Dravecz, K. Lengyel, G. Corradi. Crystals, **7** (8), 230 (2017). DOI: 10.3390/cryst7080230

Translated by A.Akhtyamov